Journal of Energy Chemistry 63 (2021) 344–350

Contents lists available at ScienceDirect

Journal of Energy Chemistry

journal homepage: www.elsevier.com/locate/jechem

http://www.journals.elsevier.com/journal-of-energy-chemistry/

Dedicated to the 100th anniversary of Chemistry at Nankai University

CO activation by the heterobinuclear transition metal-iron clusters: A photoelectron spectroscopic and theoretical study

Jumei Zhang [a,b], Zhiling Liu [c], Gang Li [a], Hongjun Fan [a], Ling Jiang [a,*], Hua Xie [a,*]

[a] State Key Laboratory of Molecular Reaction Dynamics, Dalian Institute of Chemical Physics, Chinese Academy of Sciences, Dalian 116023, Liaoning, China
[b] School of Life Science, Ludong University, Yantai 264025, Shandong, China
[c] School of Chemical and Material Science, Key Laboratory of Magnetic Molecules & Magnetic Information Materials, Ministry of Education, Shanxi Normal University, Linfen 041004, Shanxi, China

ARTICLE INFO

Article history:
Received 25 May 2021
Revised 25 June 2021
Accepted 1 July 2021
Available online 15 July 2021

Keywords:
CO activation
Metal carbonyl
Alloy surface
Photoelectron velocity-map imaging spectroscopy

ABSTRACT

Spectroscopic characterization of CO activation on multiple metal-containing catalysts remains an important and challenging goal for identifying the structure and nature of active site in many industrial processes such as Fischer-Tropsch chemistry and alcohol synthesis. Here, we use mass-selected photoelectron velocity-map imaging spectroscopy and quantum chemical calculations to study the reactions of CO molecules with several heterobinuclear transition metal-iron clusters M–Fe (M = Ti, V, Cr). The mass spectra reveal the favorable formation of $MFe(CO)_4^-$ with relatively high thermodynamic stability. The $MFe(CO)_4^-$ (M = Ti, V, Cr) complexes are established to have a metal–Fe bonded M–$Fe(CO)_4$ structure with C_{3v} geometry. While the positive charge and unpaired electrons are mainly located on the M atom, the natural charge of $Fe(CO)_4$ is about −2e. The $MFe(CO)_4^-$ (M = Ti, V, Cr) can be seen as being formed via the interactions between the M^+ fragment and the $[Fe(CO)_4]^{2-}$ core, which satisfies the 18-electron rule. The CO molecules are remarkably activated in these $MFe(CO)_4^-$. These results shed insight into the structure–reactivity relationship of heterobinuclear transition metal carbonyls and would have important implications for understanding of CO activation on alloy surfaces.

1. Introduction

The interaction of carbonyl monoxide with transition metal (TM) atom is important in many industrial processes such as hydroformylation, alcohol synthesis, and acid synthesis [1,2]. Transition metal carbonyl clusters serve as archetypical examples for demonstrating the metal–ligand and metal–metal bonding [3–6]. Elementary understanding of chemical environment for TM carbonyls in the gas phase is of great scientific and practical interest to deduce the multifaceted mechanisms of CO chemisorption on metal surfaces and the binding at active sites of catalyst. Gas-phase studies provide spectroscopic information, reaction kinetics and photophysical properties of many unsaturated transition-metal carbonyl species, which are prototypical models to study carbonyl chemisorption on the surface of a metal or the binding at active site of a catalyst. Extensive experimental and theoretical efforts have been made for mononuclear transition metal carbonyls with the emphasis on the spectroscopic and structural properties. Collision-induced dissociation [7–9], mass-selected infrared photodissociation (IRPD) spectroscopy [10–17], and photoelectron spectroscopy (PES) [18–26] are popular spectroscopic technologies to investigate the electronic structures, vibrational frequencies, bond energies of TM carbonyl clusters.

The synergy effects of two or more different transition metals in the chemical processes are expected to be responsible for high catalytic performance of heterobinuclear transition metal complexes [27]. Metal carbonyl complexes are ideal models for investigating the synergy effects of different transition metals on the catalytic performance for CO [28]. Iron carbonyls have received particular attention due to their importance in catalytic and other reactions [29]. The coordinatively-saturated homoleptic iron carbonyl $Fe(CO)_5$ has a D_{3h} structure and fulfills the 18-electron rule. The interaction of iron carbonyls with several transition metals and main group metals has been characterized experimentally. The $MFe(CO)_3^-$ (M = Sc, Y, La; U; As, Sb, Bi) carbonyls have metal–Fe bonded M–$Fe(CO)_3$ structure with C_{3v} geometry and all of the three carbonyl ligands bonded on the iron center [6,30,31]. The $CuFe(CO)_n^-$ (n = 4–7) carbonyls are determined to have $Cu(CO)_{n-4}$-$Fe(CO)_4$

* Corresponding authors.
E-mail addresses: ljiang@dicp.ac.cn (L. Jiang), xiehua@dicp.ac.cn (H. Xie).

https://doi.org/10.1016/j.jechem.2021.07.005

structures, each involving a C_{3v} symmetry $Fe(CO)_4^-$ building block [32]. The $MFe(CO)_8^+$ (M = Co, Ni, Cu) complexes are characterized to have a $M(CO)_3^+$-$Fe(CO)_5$ structures with the positive charge distributed on the $M(CO)_3$ fragement [10]. The $ZnFe(CO)_5^+$ complex has been determined to possess a Zn–$Fe(CO)_5$ structure with a Zn–Fe half bond [33]. The $PbFe(CO)_4^-$ cluster has a Pb–Fe bonded Pb–$Fe(CO)_4^-$ structure with C_{2v} geometry and all of the four carbonyl ligands bonded on the iron center [19]. Interestingly, the $BeFe(CO)_4^-$ carbonyl has a C_{3v} umbrella structure with some Be–Fe multiple bonding character involving one covalent electron-sharing s bond and two additional weak Be ← $Fe(CO)_4^-$ dative π bonding interactions, providing great insights into the metal–metal bonding between s-block elements and transition metals [34].

The synthesis of some oligomers, such as $[CdFe(CO)_4]_4$ and $[Cu_3\{Fe(CO)_4\}_3]^{3-}$, $[Cu_5\{Fe(CO)_4\}_3]^{3-}$, $[Cu_6\{Fe(CO)_4\}_3]^{3-}$, has also been achieved in the condensed phase [35–37], in which all the CO ligands are bonded to the Fe atoms while the Cd and Cu cores surrounded by the $Fe(CO)_4$ moieties. Even though the first-row early transition metals (i.e., Ti, V, Cr) are widely utilized in the industrial catalytic processes [38,39], there is no spectroscopic characterization of the reactions of CO molecules with such heterobinuclear alloys M–Fe (M = Ti, V, Cr) thus far. Herein, we report a study on the CO activation by the M–Fe (M = Ti, V, Cr) clusters. The thermodynamically stable $MFe(CO)_4^-$ complexes have been produced using a laser vaporization cluster source and probed by photoelectron velocity map imaging spectroscopy. Theoretical calculations have been carried out to understand the experimental spectral features and identify the electronic and geometrical structures of $MFe(CO)_4^-$.

2. Experimental and theoretical methods

The experiments were conducted using a homemade instrument which included a laser vaporization source and a dual-channel time-of-flight mass spectrometer. Details of the apparatus have been described elsewhere [40], and only a brief description is given below. The heterobinuclear transition metal carbonyl anions were produced by laser vaporization of M–Fe (M = Ti, V, Cr) alloys (mole ratio, M/Fe = 1:1) in the presence of a helium carrier gas seeded with 5% CO. The typical stagnation pressure of the carrier gas was about 1–5 atm. After cooling and expansion into the source chamber, the anions of interest were mass selected by a McLaren Wiley time-of-flight spectrometer and then introduced into the photodetachment region and interacted with a laser beam of 266 nm (4.661 eV). The photoelectrons were mapped onto a detector consisting of a micro-channel plate and a phosphor screen. The two-dimensional (2D) images on the phosphor screen were recorded by a charge-coupled-device (CCD) camera. Each image was obtained by accumulating 10,000–50,000 laser shots at 10 Hz repetition rate. All of the raw images were reconstructed using the basis set expansion inverse Abel transform method (BASEX) [41]. The photoelectron spectra were calibrated using the known spectrum of Au^-. The energy resolution was better than 5%, corresponding to 50 meV at electron kinetic energy (eKE) of 1 eV.

In order to elucidate the electronic and geometrical structures of $MFe(CO)_4^-$ (M = Ti, V, Cr), quantum chemical calculations were carried out using Gaussian 09 programs [42]. The 6-311+G(d) basis set was used for the C and O atoms [43], and the SDD basis set for the Ti, V, Cr, and Fe atoms [44]. To find the most appropriate functional for the $MFe(CO)_4^-$ (M = Ti, V, Cr) system, the vertical detachment energy (VDE) for the most stable structure of $TiFe(CO)_4^-$ was predicted at different density functional theory (DFT) levels and compared with the experimental data (Table S1). It turned out that the BP86/6-311+G(d)G(d)-SDD calculated VDE agrees best with the experimental value [45,46]. Thus, the BP86 functional was chosen to evaluate the electronic and geometrical properties of $MFe(CO)_4^-$ (M = Ti, V, Cr). All plausible higher spin states and structures were considered. Harmonic frequency analysis was carried out to make sure that the obtained structures were real minima on the potential energy surfaces. Theoretical calculations indicated that the lowest-lying isomers of $MFe(CO)_4^-$ (M = Ti, V, Cr) were in quartet, quintet, and sextet state, respectively. Theoretically, the VDE was calculated as the difference between the neutral and anionic species based on the optimized anion geometries, and the adiabatic detachment energy (ADE) was computed as the difference between the neutral and anionic species both at their optimized structure.

3. Results and analysis

3.1. PEs

The $MFe(CO)_4^-$ (M = Ti, V, Cr) complexes have been generated via laser vaporization of metal rods with 5% CO seeded with helium. The mass spectra of $MFe(CO)_4^-$ (M = Ti, V, Cr) are shown in Fig. 1. The mass spectra of $MFe(CO)_n^-$ (M = Ti, V, Cr) display the character of a magic number when n = 4. It is tempting to reveal that $MFe(CO)_4^-$ (M = Ti, V, Cr) are more stable than the other ones in the distribution. The photoelectron imaging results and the corresponding photoelectron spectra of $MFe(CO)_4^-$ (M = Ti, V, Cr) are displayed in Fig. 2. The raw images (upper) collected in the experiments represent the projection of the 3D laboratory-frame photoelectron probability density onto the plane of the imaging detector, and the reconstructed images (bottom) indicate the center slice of the 3D distribution from its 2D projection. The direction of laser polarization is indicated by a double arrow on each raw image.

The 266 nm spectra allow the ground-state transition to be observed for $MFe(CO)_4^-$ (M = Ti, V, Cr) and the spectra of these com-

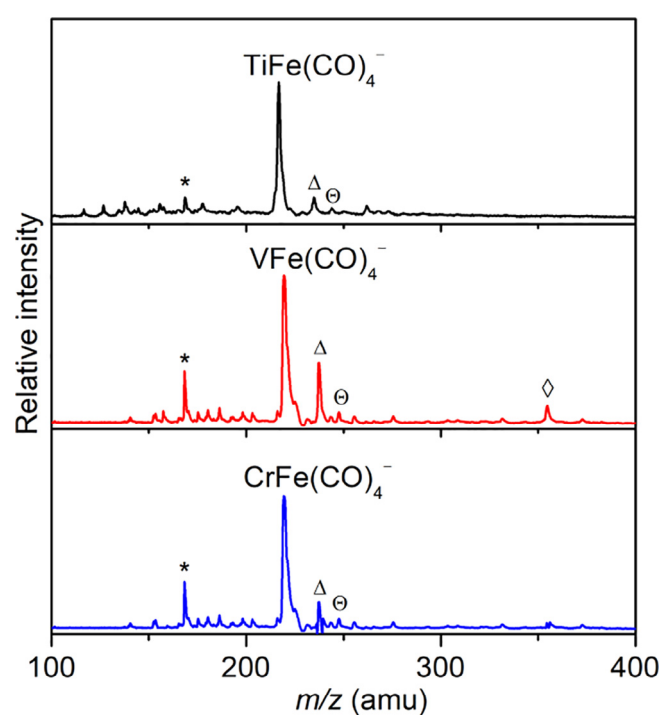

Fig. 1. Mass spectrum of heterobinuclear $MFe(CO)_4^-$ (M = Ti, V, Cr) cluster anions formed by pulsed laser vaporization of alloy metal target in an expansion of helium seeded by carbon monoxide. The mass peak labeled with "*" stands for $Fe(CO)_4^-$, "Δ" for $MFe(CO)_4(H_2O)^-$, "Θ" for $MFe(CO)_5^-$, and "◊" for $M_2Fe(CO)_4^-$.

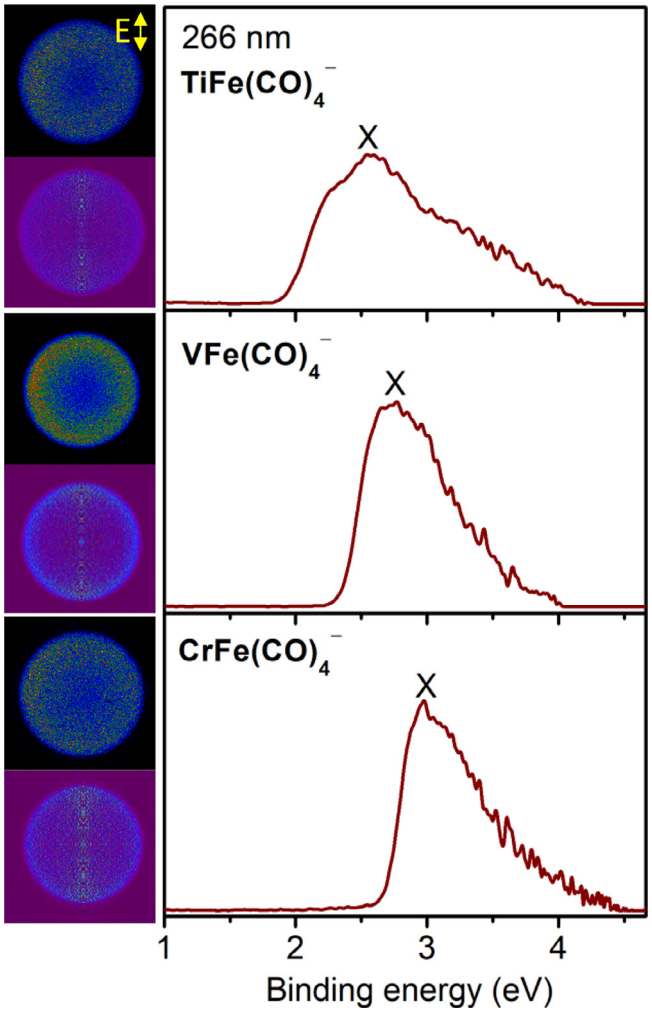

Fig. 2. Photoelectron images of $MFe(CO)_4^-$ (M = Ti, V, Cr) at 266 nm. The raw image (upper) and the reconstructed image (bottom) after inverse Abel transformation are shown on the left side. The double arrow indicates the direction of the laser polarization. Photoelectron spectra are shown on the right side.

plexes are all broad. The broad spectral features probably root from electronically and vibrationally excited anionic states generated in the hot laser vaporation cluster source. Apart from the hot cluster source, the broad band observed in the spectra may be the reasons from many other aspects, such as large geometry change upon photodetachment, coexistence of energy degenerate isomers, and congested low-lying electronic states. Among these spectra, the bandwidth of $TiFe(CO)_4^-$ is larger than the spectra of $VFe(CO)_4^-$ and $CrFe(CO)_4^-$. The measured ground-state VDEs and ADEs are listed in Table 1. The VDE values of $MFe(CO)_4^-$ (M = Ti, V, Cr) are 2.49 ± 0.11, 2.75 ± 0.10, 2.97 ± 0.08 eV, respectively, showing an increase trend with the atomic number. The ADE values are estimated by drawing a straight line at the rising edge of the main band. The ADE values of $MFe(CO)_4^-$ (M = Ti, V, Cr) are evaluated to be 2.20 ± 0.12, 2.32 ± 0.12, 2.58 ± 0.10 eV, respectively.

3.2. Comparison between experimental and theoretical results

Quantum chemical calculations were carried out to elucidate the geometric and electronic structures and support the spectral assignments. The optimized structures of the four lowest-energy isomers for $MFe(CO)_4^-$ (M = Ti, V, Cr) are displayed in Fig. 3. The optimized structures of the higher-energy isomers for $MFe(CO)_4^-$ (M = Ti, V, Cr) are shown in Figs. S1–S3, respectively. The calculated VDE and ADE values of the four lowest-energy isomers are listed in Table 1. The previous experimental and calculated studies have indicated that the lowest-lying structure for $Fe(CO)_4^-$ is a C_{3v} symmetry with $^2A_1$ ground state [47–49]. The experimental VDE and ADE values of $Fe(CO)_4^-$ are 2.94 ± 0.03 and 2.53 ± 0.05 eV (Fig. S4), respectively, which agree well with the experimental observations reported previously [50].

$TiFe(CO)_4^-$. The lowest-lying isomer of $TiFe(CO)_4^-$ labeled as **4A** is a C_{3v} structure with $^4A_1$ electronic state with the Ti atom and four CO terminally bonded to the Fe atom. The calculated VDE and ADE values of **4A** are 2.41 and 2.13 eV, respectively, which is in excellent agreement with the experimental VDE and ADE values (2.49 ± 0.11 and 2.20 ± 0.12 eV). The **4B** isomer is 0.18 eV higher in energy than **4A**, which includes three CO terminally bonded to the Fe atom and one CO terminally bonded to the Ti atom. The **4B** isomer is a C_s structure with $^4A'$ electronic state. The calculated VDE and ADE are 2.37 and 2.12 eV, respectively, which is also in agreement with the experimental values. The **4C** isomer is 0.24 higher in energy than **4A**, which is in $^2A_1$ and contains four terminal CO bonded to the Fe atom. The calculated VDE and ADE values of **4C** are 2.01 and 1.89 eV, respectively, which is much lower than the experimental data. The VDE and ADE values of **4C** isomer cannot fit well with the experimental values. The **4D** isomer is in $^2A'$ electronic state which includes three bridging CO and one terminal CO bonded to Fe. The **4D** isomer is 0.68 eV higher in energy than **4A**, and it should be too high in energy to be probed in the experiment. From the current experimental condition, **4A** and **4B** are probably the main isomers present in the experiment.

$VFe(CO)_4^-$. For $VFe(CO)_4^-$, the lowest-energy structure labeled as **4a** is a C_{3v} structure with a $^5A_1$ electronic state, which could be built from the $Fe(CO)_5$ by exchange of one equatorial carbonyl group by a vanadium atom, which is similar to the **4A** structure of $TiFe(CO)_4^-$. While the **4b** structure has a C_{2v} symmetry with $^5A_1$ electronic state, which a V atom and four CO terminally bonded to Fe atom. The **4b** isomer is 0.04 eV higher in energy than **4a**. The **4c** isomer (+0.39 eV) is in $^5A'$ electronic state which includes three CO terminally bonded to the Fe atom and one CO terminally bonded to a V atom. The **4d** isomer is 0.59 eV higher than **4a**, which is in $^3A_1$ and can be viewed as a V atom and four CO terminally bonded to a Fe atom. The calculated VDE and ADE values of **4a** (2.67 and 2.27 eV) match well with the experiment values (2.75 ± 0.10 and 2.32 ± 0.12 eV). The calculated VDE of **4b** is slightly different from the experimental value. The **4c** and **4d** isomers can be excluded because they are too high in energy than **4a** and their VDE and ADE values cannot fit well with the experimental values.

$CrFe(CO)_4^-$. The most stable structure **4-I** has C_{3v} symmetry with a $^6A_1$ electronic state. All of the CO molecules are bonded to the Fe atom and the **4-I** structure can be considered as a Cr atom bonded to Fe center of iron tetracarbonyl. The **4-II** isomer (+0.92 eV) has C_{3v} symmetry with a $^6A_1$ electronic state, which includes one terminal CO bonded to Cr and three carbonyls terminally bonded to Fe. The **4-III** isomer is 0.98 eV higher in energy than **4A**, which has C_{2v} symmetry with a $^4A_1$ electronic state and can be seen as built from the tetra-carbonyl chromium by bonding additional Fe atoms on the centric Cr atom. The **4-IV** isomer is 1.00 eV in energy higher than **4-I**, which has C_{2v} symmetry with a $^4A_1$ electronic state. Moreover, it contains a Cr atom and four CO terminally bonded to the Fe atom. The calculated VDE and ADE values of **4-I** (3.04 and 2.49 eV) fit well with the experimental values (2.97 ± 0.08 and 2.58 ± 0.10 eV), while isomers **4-II**, **4-III**, and **4-IV** are too high in energies to exist in the current experimental conditions. The existence of only one structure in the experimental observation gives rise to the relative narrower spectrum of $CrFe(CO)_4^-$.

Table 1
Comparison of experimental VDE and ADE values to BP86/6-311+G(d)G(d)-SDD calculated ones of the four lowest-energy isomers for $MFe(CO)_4^-$ (M = Ti, V, Cr).

Cluster	Isomer	Relative energy (eV)	VDE		ADE	
			Expt.[a]	Calc.	Expt.[a]	Calc.
$TiFe(CO)_4^-$	**4A**	0.00	2.49(11)	2.41	2.20(12)	2.13
	4B	0.18		2.37		2.12
	4C	0.24		2.01		1.89
	4D	0.68		2.56		2.40
$VFe(CO)_4^-$	**4a**	0.00	2.75(10)	2.67	2.32(12)	2.27
	4b	0.04		2.50		2.24
	4c	0.39		2.43		2.19
	4d	0.59		1.87		1.69
$CrFe(CO)_4^-$	**4-I**	0.00	2.97(8)	3.04	2.58(10)	2.49
	4-II	0.92		2.88		2.39
	4-III	0.98		3.00		2.65
	4-IV	1.00		1.58		1.49

[a] Numbers in parentheses represent the uncertainty in the last digit.

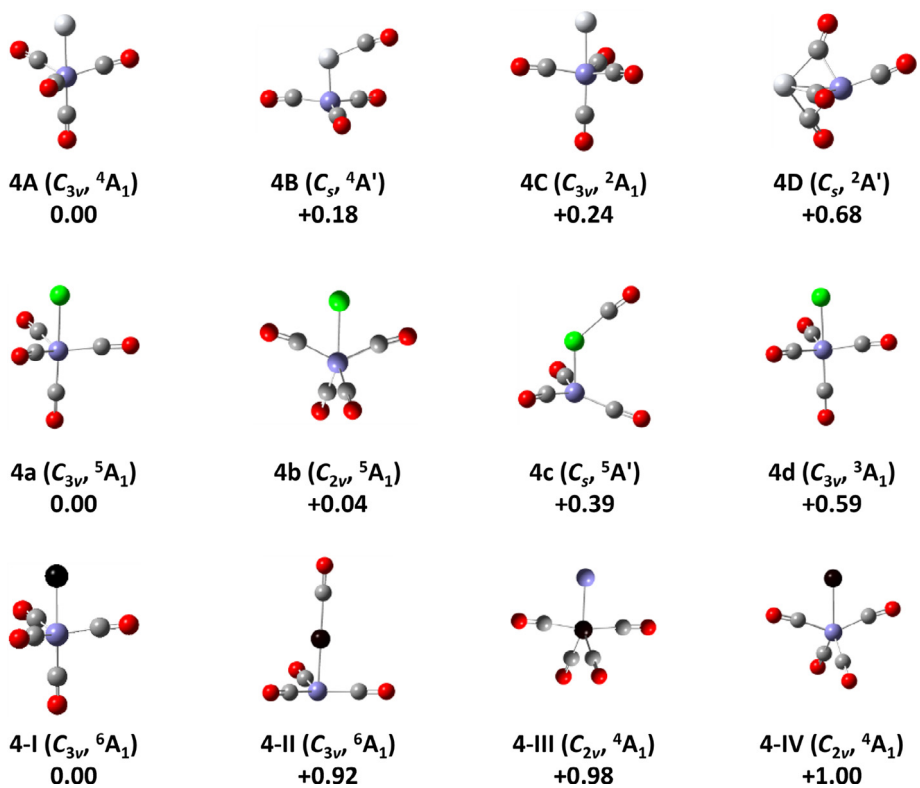

Fig. 3. Optimized structures of the four lowest-energy isomers for $MFe(CO)_4^-$ (M = Ti, V, Cr) (Ti, light gray; V, green; Cr, black; Fe, purple; C, gray; O, red). Relative energies are given in eV.

4. Discussion

On the basis of the good consistency between experimental and theoretical results, the structures of the $MFe(CO)_4^-$ (M = Ti, V, Cr) complexes are established to be trigonal bipyramidal with all the CO terminally bonded to the Fe atom and the M atom bonded to Fe center of iron tetracarbonyl. Previous studies indicated that $PbFe(CO)_4^-$, $CdFe(CO)_4^-$, $ZnFe(CO)_4^-$, and $HgFe(CO)_4^-$ all possessed iron tetracarbonyl anion structures [19,35,51], implying that the isomers $MFe(CO)_4^-$ with iron tetracarbonyl anion configuration are stable. Natural population analysis (Table 2) shows that the positive charge and unpaired electrons are largely located on the M atom and the natural charge of $Fe(CO)_4$ is about −2e. Mulliken population analysis shows that the spin densities are mainly located on M with Ti(3.11), V(4.23), and Cr(5.33). The electron transfers from the M atom to the Fe atom, which leads to M (I) formal oxidation state and Fe(-II) formal oxidation state. Therefore, the $MFe(CO)_4^-$ (M = Ti, V, Cr) complexes can be seen as being formed via the interactions between the M^+ fragment and the $[Fe(CO)_4]^{2-}$, which satisfy the 18-electron rule and are in accord with the feature of $MFe(CO)_4^-$ (M = Ti, V, Cr) dominated in the mass spectra. The M–Fe bond distance is predicted to be 2.42, 2.39, and 2.44 Å, respectively, which trend is in line with the previous report [4]. The M–Fe bond in these cluster anions can be regarded as a formal single bond.

The high spin states of $MFe(CO)_4^-$ (M = Ti, V, Cr) are more favorable than low spin states. The most stable structures of $MFe(CO)_4^-$ (M = Ti, V, Cr) are characterized to have quartet, quintet, and sextet electronic states, respectively. The coexistences of isomers for $TiFe(CO)_4^-$ are in accord with the broad peak observed in the spectrum.

Table 2
M–Fe bond lengths, wiberg bond orders and natural charges of $MFe(CO)_4^-$ (M = Ti, V, Cr) species calculated at the BP86/6-311+G(d)G(d)-SDD level of theory.

Species	M–Fe bond length (Å)	M–Fe wiberg bond order	Natural charge	
			M	Fe
$TiFe(CO)_4^-$	2.42	0.67	0.42	−2.05
$VFe(CO)_4^-$	2.39	0.64	0.37	−2.05
$CrFe(CO)_4^-$	2.44	0.52	0.38	−2.08

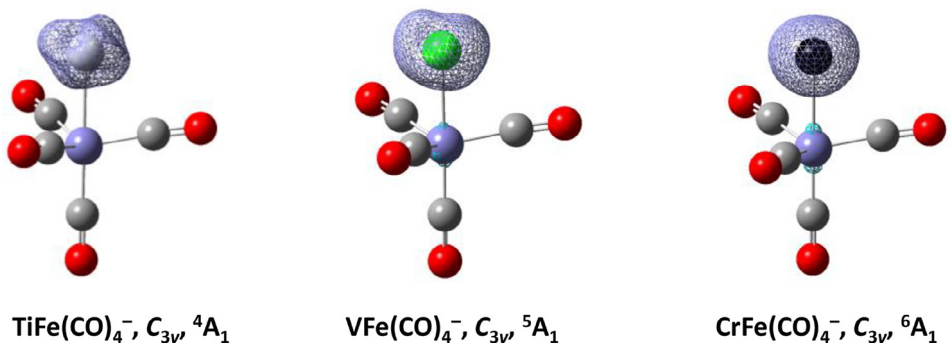

Fig. 4. Isosurface map of unpaired spin density distributions for $MFe(CO)_4^-$ (M = Ti, V, Cr) calculated at the BP86/6-311+G(d)G(d)-SDD level of theory.

The existence of single isomer for $VFe(CO)_4^-$ and $CrFe(CO)_4^-$ leads to the relative sharper spectra. The isosurface map of unpaired spin density distributions for $MFe(CO)_4^-$ (M = Ti, V, Cr) (Fig. 4) shows that almost spin densities are located on the M atom. The contributions of the unpaired spin density distributions for Ti, V, Cr in the $MFe(CO)_4^-$ (M = Ti, V, Cr) species are listed in Table 3. For $TiFe(CO)_4^-$, the spin density is mostly located on Ti center (3.11) with 4*s* orbital contribution of 21%, 4*p* contribution of 4%, 3*d* contribution of 75%. The spin density of $VFe(CO)_4^-$ is almost located on V center (4.23), with 4*s*/4*p*/3*d* contribution of 13%, 5%, and 82%, respectively. For $CrFe(CO)_4^-$, the spin density is mostly located on Cr center (5.33) with 4*s* orbital contribution of 10%, 4*p* contribution of 3%, 3*d* contribution of 87%. The 4*s* contribution for the unpaired spin density of Ti in the $TiFe(CO)_4^-$ is more than that of V and Cr in the $VFe(CO)_4^-$ and $CrFe(CO)_4^-$. The VDE of $MFe(CO)_4^-$ (M = Ti, V, Cr) is increasing with 3*d* contribution increasing and 4*s* contributions decreasing.

Table 3
Contributions of the unpaired spin density distributions for Ti, V, Cr in the $MFe(CO)_4^-$ (M = Ti, V, Cr) species.

Species	Spin density of M	4*s*	4*p*	3*d*
$TiFe(CO)_4^-$	3.11	21%	4%	75%
$VFe(CO)_4^-$	4.23	13%	5%	82%
$CrFe(CO)_4^-$	5.33	10%	3%	87%

Fig. 5 shows the highest occupied molecular orbitals (HOMO) of the most stable isomers for $MFe(CO)_4^-$ (M = Ti, V, Cr) down to the sixth valence molecular orbital from the HOMO. The orbital composition analyses by natural atomic orbital (NAO) method to the frontier KS-MOs of these species are shown in the Tables S2–S4, respectively. The HOMO and HOMO-1 of $TiFe(CO)_4^-$ are singly occupied orbitals, which are virtually non-bonding titanium-based 3*d*

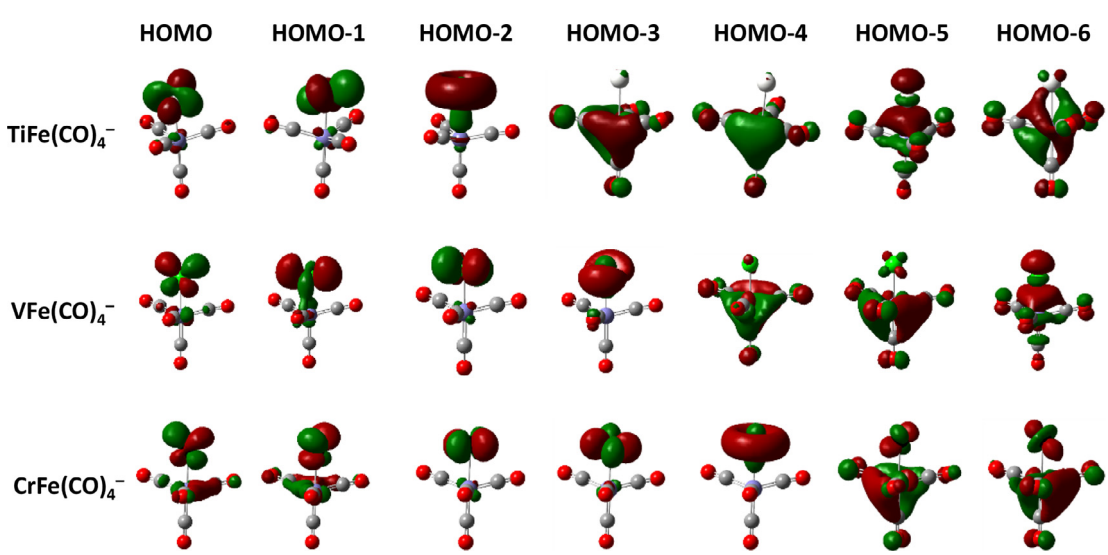

Fig. 5. Molecular orbital pictures of the most stable isomers for $MFe(CO)_4^-$ (M = Ti, V, Cr) calculated at the BP86/6-311+G(d)G(d)-SDD level of theory, showing the HOMO down to the sixth valence molecular orbital from the HOMO.

orbitals with the 3*d* orbitals contributing about 90%. While the HOMO-2 of $TiFe(CO)_4^-$ is also singly occupied orbital, which is made up of a non-bonding orbital with 3*d*/4*s*/4*p* orbitals contributing 35%/47%/12%, respectively. The next two doubly occupied molecular orbitals (HOMO-3 and HOMO-4) of $TiFe(CO)_4^-$ are nearly degenerate, primarily Fe 3*d* orbitals, which comprise notable Fe to CO $2\pi^*$ back-donation. The doubly occupied HOMO-5 of $TiFe(CO)_4^-$ is a Ti–Fe σ bonding orbital, which is stemmed from combination of Fe 3*d* and 4*p* hybrid orbitals (13% 3*d* + 30% 4*p*) and Ti 3*d* and 4*s* hybrid orbitals (8% 3*d* + 18% 4*p*). The doubly occupied HOMO-6 orbital comprises primarily Fe 3*d* orbital (72% 3*d*). While for $VFe(CO)_4^-$, HOMO, HOMO-1, HOMO-2, HOMO-3 orbitals are singly occupied orbitals, which are non-bonding vanadium-based 3*d* orbitals, with the 3*d* contribution 83%, 72%, 95% and 65%, respectively. The next two doubly occupied molecular orbitals (HOMO-4 and HOMO-5) of $VFe(CO)_4^-$ are nearly degenerate, which comprise notable Fe to CO $2\pi^*$ back-donation. The doubly occupied HOMO-6 orbital of $VFe(CO)_4^-$ is a V–Fe σ bonding orbital, which results from combination of Fe 3*d* and 4*p* hybrid orbitals (27% 3*d* + 13% 4*p*) and V 3*d* and 4*s* hybrid orbitals (16% 3*d* + 17% 4*p*). For $CrFe(CO)_4^-$, the singly occupied HOMO, HOMO-1, HOMO-2, HOMO-3 and HOMO-4 orbitals are non-bonding chromium-based 3*d* orbitals with the 3*d* contribution 70%, 70%, 96%, 96% and 65%, respectively. The doubly occupied HOMO-5 and HOMO-6 orbitals are degenerate, which comprise Fe to CO $2\pi^*$ back-donation.

The C–O bond distances in the $MFe(CO)_4^-$ (M = Ti, V, Cr) complexes were calculated to be about 1.18 Å at the BP86/6-311+G(d)G(d)-SDD level of theory (Fig. S5), which are longer than that of the free CO molecule (1.13 Å). The corresponding CO stretching frequencies were predicted to be in the 1810–1920 cm^{-1} region, which are remarkably redshifted from that of the free CO molecule (2121 cm^{-1} at the same theory level). These results suggest that the C–O bonds are weakened in these $MFe(CO)_4^-$ complexes as compared to that in the free CO molecule. Indeed, the C–O bond weakening has been reported for chemisorbed CO on various transition metal surfaces [38], for which the CO stretching frequencies appear around 1100–2000 cm^{-1}. Along with the advances in various experimental and theoretical efforts, these studies would have important implications for understanding the CO activation and relevant processes on metal catalysts.

5. Conclusions

The heterobinuclear metal-iron carbonyl anions $MFe(CO)_4^-$ (M = Ti, V, Cr) have been generated via a laser vaporization supersonic cluster source and characterized by mass-selected photoelectron velocity-map imaging spectroscopy. Quantum chemical calculations have been carried out to elucidate the geometric and electronic structures. The signal intensity of $n = 4$ in the mass spectra of $MFe(CO)_n^-$ is more intense than other species, revealing a higher thermodynamic stability of the target products. The $MFe(CO)_4^-$ complexes are characterized to possess trigonal bipyramidal structures with all the CO terminally bonded to the Fe atom and with the M atom bonded to the Fe center of iron tetracarbonyl. The positive charge and unpaired electrons are mainly located on the M atom. The natural charge of $Fe(CO)_4$ is about −2e. The $MFe(CO)_4^-$ (M = Ti, V, Cr) can be seen as being formed via the interactions between the M^+ fragment and the $[Fe(CO)_4]^{2-}$, which satisfy the 18-electron rule and are in accord with the experimental features. The C–O bonds are apparently weakened in these $MFe(CO)_4^-$. The present results would advance the understanding of chemisorbed CO molecules on alloy surfaces and help to refine the appropriate CO activation via the selection of different transition metals and metal compounds.

Declaration of Competing Interest

The authors declare that they have no known competing financial interests or personal relationships that could have appeared to influence the work reported in this paper.

Acknowledgments

This work was supported by the National Natural Science Foundation of China (21688102, 21873097, and 92061203), the Youth Innovation Promotion Association of the Chinese Academy of Sciences (CAS) (2020187), the Strategic Priority Research Program of CAS (XDB17000000), CAS (GJJSTD20190002), the International Partnership Program of CAS (121421KYSB20170012), and the K.C. Wong Education Foundation (GJTD-2018-06).

Appendix A. Supplementary data

Supplementary data to this article can be found online at https://doi.org/10.1016/j.jechem.2021.07.005.

References

[1] E.L. Muetterties, J. Stein, Chem. Rev. 79 (1979) 479–490.
[2] W. Tumas, B. Gitlin, A.M. Rosan, J.T. Yardley, J. Am. Chem. Soc. 104 (1982) 55–59.
[3] L. Pauling, Proc. Natl. Acad. Sci. U.S.A. 73 (1976) 4290–4293.
[4] G. Frenking, N. Frohlich, Chem. Rev. 100 (2000) 717–774.
[5] P. Macchi, A. Sironi, Coord. Chem. Rev. 238 (2003) 383–412.
[6] J.Q. Wang, C.X. Chi, H.S. Hu, L.Y. Meng, M.B. Luo, J. Li, M.F. Zhou, Angew. Chem. Int. Ed. 57 (2018) 542–546.
[7] X.G. Zhang, P.B. Armentrout, Organometallics 20 (2001) 4266–4273.
[8] L.S. Sunderlin, D.N. Wang, R.R. Squires, J. Am. Chem. Soc. 114 (1992) 2788–2796.
[9] F. Meyer, Y.M. Chen, P.B. Armentrout, J. Am. Chem. Soc. 117 (1995) 4071–4081.
[10] H. Qu, F.C. Kong, G.J. Wang, M.F. Zhou, J. Phys. Chem. A 120 (2016) 7287–7293.
[11] H.A. Abdulhussein, P. Ferrari, J. Vanbuel, C. Heard, A. Fielicke, P. Lievens, E. Janssens, R.L. Johnston, Nanoscale 11 (2019) 16130–16141.
[12] P. Ferrari, J. Vanbuel, T. Nguyen Minh, N. Minh Tho, S. Gewinner, W. Schoellkopf, A. Fielicke, E. Janssens, Chem. Eur. J. 23 (2017) 4120–4127.
[13] A.D. Brathwaite, M.A. Duncan, J. Phys. Chem. A 117 (2013) 11695–11703.
[14] A.D. Brathwaite, Z.D. Reed, M.A. Duncan, J. Phys. Chem. A 115 (2011) 10461–10469.
[15] M.F. Zhou, L. Andrews, J. Phys. Chem. A 103 (1999) 6956–6968.
[16] A.M. Ricks, Z.E. Reed, M.A. Duncan, J. Mol. Spectrosc. 266 (2011) 63–74.
[17] I. Swart, F.M.F. de Groot, B.M. Weckhuysen, D.M. Rayner, G. Meijer, A. Fielicke, J. Am. Chem. Soc. 130 (2008) 2126–2127.
[18] Z.L. Liu, H. Xie, Z.B. Qin, H.J. Fan, Z.C. Tang, Inorg. Chem. 53 (2014) 10909–10916.
[19] Z.L. Liu, J.H. Zou, Z.B. Qin, H. Xie, H.J. Fan, Z.C. Tang, J. Phys. Chem. A 120 (2016) 3533–3538.
[20] J.E. Reutt, L.S. Wang, Y.T. Lee, D.A. Shirley, Chem. Phys. Lett. 126 (1986) 399–404.
[21] J.H. Zou, H. Xie, Q.Q. Yuan, J.M. Zhang, D.X. Dai, H.J. Fan, Z.C. Tang, L. Jiang, Phys. Chem. Chem. Phys. 19 (2017) 9790–9797.
[22] G. Li, J.M. Zhang, H. Xie, X.T. Kong, L. Jiang, J. Phys. Chem. A 122 (2018) 3811–3818.
[23] J.M. Zhang, H. Xie, G. Li, X.T. Kong, H.J. Fan, L. Jiang, J. Phys. Chem. A 122 (2018) 53–59.
[24] H. Xie, J.H. Zou, Q.Q. Yuan, J.M. Zhang, H.J. Fan, L. Jiang, Top. Catal. 61 (2018) 71–80.
[25] J.M. Zhang, G. Li, Q.Q. Yuan, J.H. Zou, D. Yang, H.J. Zheng, C. Wang, J.P. Yang, Q.S. Jing, Y.M. Liu, H.J. Fan, H. Xie, J. Phys. Chem. A 124 (2020) 2264–2269.
[26] E.F. van der Eide, G.L. Hou, S.H.M. Deng, H. Wen, P. Yang, R.M. Bullock, X.B. Wang, Organometallics 32 (2013) 2084–2091.
[27] S. Komiya, Coord. Chem. Rev. 256 (2012) 556–573.
[28] G. Gervasio, E. Sappa, A. Secco, J. Organomet. Chem. 751 (2014) 111–152.
[29] G.W. Parshall, S.D. Ittel, Homogeneous Catalysis, second ed., Wiley, New York, 1992.
[30] J.Q. Wang, C.X. Chi, H.S. Hu, X. Li, M.B. Luo, J. Li, M.F. Zhou, Angew. Chem. Int. Ed. 59 (2020) 2344–2348.
[31] C.X. Chi, J.Q. Wang, H. Qu, W.L. Li, L.Y. Meng, M.B. Luo, J. Li, M.F. Zhou, Angew. Chem. Int. Ed. 56 (2017) 6932–6936.
[32] N. Zhang, M.B. Luo, C.X. Chi, G.J. Wang, J.M. Cui, M.F. Zhou, J. Phys. Chem. A 119 (2015) 4142–4150.
[33] H. Qu, F.C. Kong, G.J. Wang, M.F. Zhou, J. Phys. Chem. A 121 (2017) 1628–1633.
[34] G.J. Wang, J. Zhao, H.S. Hu, J. Li, M.F. Zhou, Angew. Chem. Int. Ed. 60 (2021) 9334–9338.
[35] R.D. Ernst, T.J. Marks, J.A. Ibers, J. Am. Chem. Soc. 99 (1977) 2090–2098.

[36] G. Doyle, K.A. Eriksen, D. Vanengen, J. Am. Chem. Soc. 108 (1986) 445–451.
[37] G. Doyle, K.A. Eriksen, D. Vanengen, J. Am. Chem. Soc. 107 (1985) 7914–7920.
[38] H.J. Freund, G. Meijer, M. Scheffler, R. Schlogl, M. Wolf, Angew. Chem. Int. Ed. 50 (2011) 10064–10094.
[39] R.H.D. Lyngdoh, H.F. Schaefer III, R.B. King, Chem. Rev. 118 (2018) 11626–11706.
[40] Z.B. Qin, X. Wu, Z.C. Tang, Rev. Sci. Instrum. 84 (2013) 066108.
[41] V. Dribinski, A. Ossadtchi, V.A. Mandelshtam, H. Reisler, Rev. Sci. Instrum. 73 (2002) 2634–2642.
[42] M.J. Frisch, G.W. Trucks, H.B. Schlegel, G.E. Scuseria, M.A. Robb, J.R. Cheeseman, G. Scalmani, V. Barone, B. Mennucci, G.A. Petersson, H. Nakatsuji, M. Caricato, X. Li, H.P. Hratchian, A.F. Izmaylov, J. Bloino, G. Zheng, J.L. Sonnenberg, M. Hada, M. Ehara, K. Toyota, R. Fukuda, J. Hasegawa, M. Ishida, T. Nakajima, Y. Honda, O. Kitao, H. Nakai, T. Vreven, J.A. Montgomery Jr., J.E. Peralta, F. Ogliaro, M.J. Bearpark, J. Heyd, E.N. Brothers, K.N. Kudin, V.N. Staroverov, R. Kobayashi, J. Normand, K. Raghavachari, A.P. Rendell, J.C. Burant, S.S. Iyengar, J. Tomasi, M. Cossi, N. Rega, N.J. Millam, M. Klene, J.E. Knox, J.B. Cross, V. Bakken, C. Adamo, J. Jaramillo, R. Gomperts, R.E. Stratmann, O. Yazyev, A.J. Austin, R. Cammi, C. Pomelli, J.W. Ochterski, R.L. Martin, K. Morokuma, V.G. Zakrzewski, G.A. Voth, P. Salvador, J.J. Dannenberg, S. Dapprich, A.D. Daniels, O. Farkas, J.B. Foresman, J.V. Ortiz, J. Cioslowski, D.J. Fox, Gaussian 09, Gaussian Inc, Wallingford, CT, USA, 2009.
[43] R. Krishnan, J.S. Binkley, R. Seeger, J.A. Pople, J. Chem. Phys. 72 (1980) 650–654.
[44] M. Dolg, U. Wedig, H. Stoll, H. Preuss, J. Chem. Phys. 86 (1987) 866–872.
[45] A.D. Becke, Phys. Rev. A 38 (1988) 3098–3100.
[46] J.P. Perdew, Phys. Rev. B 33 (1986) 8822–8824.
[47] A. Ricca, C.W. Bauschlicher Jr., J. Phys. Chem. A 99 (1995) 5922–5926.
[48] M.F. Zhou, L. Andrews, J. Chem. Phys. 111 (1999) 10370.
[49] G.J. Wang, C.X. Chi, J.M. Cui, X.P. Xing, M.F. Zhou, J. Phys. Chem. A 116 (2012) 2484–2489.
[50] P.C. Engelking, W.C. Lineberger, J. Am. Chem. Soc. 101 (1979) 5569–5573.
[51] R.D. Ernst, T.J. Marks, Inorg. Chem. 17 (1978) 1477–1484.